Chapter 4

Experimental Results and Discussion

In this chapter, the characteristics of VCSELs with various device sizes are discussed. Changes in the active region diameter affect the electrical and thermal properties of VCSELs. The associated parameters, such as threshold current, threshold current density, maximum output power, serious resistance, temperature of active region and thermal impedance, scale differently with device size resulting in changes in performance metrics. Therefore, the main purpose of our experiment is to compare the variations of electrical and thermal properties with different active region sizes. A variety of active region sizes for our VCSEL devices analyzed in the following sections were fabricated on the sample with photoresist implant mask nominal diameters of 10, 12, 15, and 20 μm.

This chapter is organized as follows. First, the dependence of VCSEL performance such as series resistance, threshold current, threshold current density, and output power is discussed. The slope efficiency and wall-plug efficiency are also described. Second, the influence of spatial hole burning and self-focusing effect on the transverse modes of VCSELs is studied. Then, the phenomenon of the kink in L-I curve is also investigated. Finally, the thermal roll-over effect, active region temperature, and the dependence of threshold current as well as output power on the temperature of laser cavity are investigated.

4.1 The CW L-I-V Characteristics

Figure 4.1 shows typical L-I-V characteristics of a VCSEL. The labels “1”, “2”, “3”, “4”, “5”represent threshold current, series resistance, maximum output power, slope efficiency, and operating current range, respectively. With these parameters, we could estimate the

wall-plug efficiency.

4.1.1 The Dependence of VCSEL Performance on Device Size

The continuous wave I-V characteristics of the VCSEL devices are shown in Figure 4.2, and the measured device resistance with cross-sectional areas defined by proton implantation is shown in Figure 4.3. The device resistance was taken from a linear fit of the current versus voltage curves in Figure 4.2 between the lasing threshold and maximum output power points on the curves. The current versus voltage relationship is quite linear in this range. The data for resistance dependence on device sizes can be further analyzed by fitting it to the empirical formula【36】,

$$R_S = \frac{R_L}{r} + \frac{R_V}{\pi r^2} \qquad \textbf{(4.1)}$$

where R_L is the lateral resistance fitting coefficient, R_V is the vertical resistance fitting coefficient, and r is the active region radius. The first term accounts for constriction or spreading, lateral, and contact resistances that scales inversely with active region radius. The second term varies inversely with active region area to reflect voltage drops associated with uniform vertical current flow through the mirror. The best fit is obtained with coefficient values of $R_L = 2\times10^{-2}\ \Omega\text{-cm}$ and $R_V = 1.8\times10^{-4}\ \Omega\text{-cm}^2$.

As above-mentioned, the series resistance is primarily due to the vertical resistance of p-type DBRs. In addition, fabrication also influences the lateral resistance of annular contacted VCSEL structures. Damage caused by proton implantation increases both bulk and contact resistivity. Hence, this highlights the importance of enhancing vertical as well as lateral conductivity in VCSEL mirror stacks.

The continuous wave L-I characteristics of the VCSEL devices are shown in Figure 4.4. The threshold current density and threshold current against the active region area are shown in Figure 4.5. Ideally, in the absence of edge effects and current crowding, the threshold current

density should keep relatively constant giving a threshold current that is proportional to the active region area. However, it is observed that the threshold current density increases with the decrease in the area of active region in Figure 4.5. This is partly due to effects that require additional currents which scale with the device circumference, such as nonradiative recombination that occurs at the periphery of the implant. Though the threshold current density increases as the active region area is reduced, the variation of threshold current density between various active region areas is small. We could regard the threshold current densities as nearly uniform. Therefore, the data in Figure 4.5 shows that the threshold current is approximately proportional to the active region area.

Figure 4.6 shows two performance metrics, operating current range and maximum output power, as functions of the device size. It is observed that the current range and maximum output power are reduced with device size. Several effects are responsible for the reduction of operating current and output power as device size is reduced: (1) the thermal resistance of VCSELs, which is inversely proportional to device size i.e., small devices suffer high thermal dissipation; (2) the size dependence of cavity loss due to the surface scattering and diffraction losses; and (3) the increase in threshold current density with the junction temperature.

4.1.2 Slope Efficiency and Wall-Plug Efficiency

Slope efficiency is the increase of output power divided by the increase of current injection. So a VCSEL device with good current to light inversion speed has a good performance, and this performance is reflected in the slope efficiency. Before the power-saturation mechanisms set in, the slope dP/dI is reasonably constant. Hence, we can acquire the slope efficiency of VCSEL devices by extracting the slope of the L-I curves in Figure 4.2. On the other hand, we can calculate the wall-plug efficiency for analysis of overall conversion efficiency between electrical and optical power is defined as【37】

$$\eta_{wp} = \frac{P}{I^2 R_S + I V_J} \quad \textbf{(4.2)}$$

where P is the output optical power, I is the injection current, R_S is the series resistance, and V_J is the voltage dropped internally in the laser junction. Wall-plug efficiency could be used to level the performance of VCSELs. Low threshold current and high slope efficiency are the basic requirements to achieve low power consuming. The slope efficiency and wall-plug efficiency of various device sizes are listed as follow:

Diameter of active region	10μm	12μm	15μm	20μm
Slope Efficiency (mW/mA)	0.258	0.11	0.155	0.168
Maximum Wall-Plug Efficiency (%)	2.05	1.43	2.23	2.78

4.2 Transverse Mode Behavior

The transverse mode dynamics are strongly dependent on the spatial carrier distribution, which itself is governed by the influence of pump-induced current spreading, spatial hole burning (SHB), and thermal gradients in the laser cavity. In the following paragraphs, the influence of SHB and self-focusing effect due to thermal lensing on the transverse modes is discussed. In addition, the phenomenon of the kink in L-I curve is also investigated.

4.2.1 Influence of Spatial Hole Burning (SHB) and Self-Focusing Effect on the Transverse Modes

Although VCSELs operate in single longitudinal mode, there are often many transverse modes competing at large bias current, which can have dramatic effects on the static and dynamic behaviors of VCSELs. This mode competition causes both spatial and temporal fluctuations in the intensity of the emitted light. The appearance and coexistence of these

transverse modes can be due to non-uniform current injection or spatial hole burning (SHB). SHB is the inhomogeneous carrier distribution due to an inhomogeneous photon distribution. In the region with a high photon density, the locally higher stimulated recombination will deplete the carriers. In order to maintain the threshold gain necessary for lasing, the carrier density will increase in the adjacent regions with lower intensity, creating a “hole” in the carrier distribution, as illustrated in Figure 4.7. For VCSELs operating at high power, SHB will reduce the modal gain of the fundamental mode so that higher order transverse mode can be excited. This is due to the reduction of overlap between the transverse distribution of optical gain and the fundamental mode. On the contrary, overlap between the transverse distribution of optical gain and side-mode will increase, leading to a mode-jump or multimode operation.

For gain-guided VCSELs under CW operation, active region heating results in a non-uniform, bell-shaped temperature distribution, and the temperature distribution becomes more pronounced with the increasing pump current. Hence, the refractive index at the radiation regions increases due to the increases in temperature, i.e., $\partial n/\partial T > 0$, causing the focus of the radiation fields. The profile of the transverse modes will be collimated to the center of the active region and the corresponding modal gain will be varied. This self-focusing of the transverse modes into the core region of the active layer is well-known as thermal lensing. Furthermore, the self-focusing effect will be amplified by SHB because of the carrier induced index change through the series SHB. The refractive index is inversely proportional to the carrier density, i.e., $\partial n/\partial N < 0$. The consequence of self-focusing due to thermal lensing and SHB is the reduction of threshold gain of the higher order transverse modes, which can be excited at lower injection levels. In other words, the self-focusing effect increases the modal gain of high order modes and suppresses the domination of the fundamental mode. Hence, the self-focusing effect can have a significant influence on the stability of transverse modes of VCSELs. The scheme of self-focusing effect is shown in

Figure 4.8(a).

In addition, a “kink” occurred in the L-I curves as illustrated in Figure 4.8(b), which indicates the onset of higher order transverse modes. This phenomenon is usually observed in gain-guided devices because the active layer has no built-in refractive index profile to confine the transverse modes so that any variation of refractive index profile will change the transverse mode profile or excite higher order transverse modes.

4.2.2 Kink and Slope Efficiency in L-I Curve

The kink phenomenon is clearly observed from the slope efficiencies in the L-I curve at various current points. Figure 4.9 shows the slope efficiency in relation to the kinks in the L-I curve of a 12 μm diameter VCSEL. In Figure 4.9, it is observed that the magnitude of slope increases to a local maximum regularly above threshold current, and then it suddenly drops at the place corresponding to the kink. This phenomenon can be explained that the light intensity of the fundamental mode increases continuously above threshold current, and then the power saturates noticed by the decreasing magnitude of slope at the place of the kink due to mode shrinkage for self-focusing effect. After that, the magnitude of slope increases from a local minimum to another local maximum again, and it implies the generation of the first high order mode with additional power contribution.

Figure 4.10 shows the emission spectra in the vicinity of the kink in L-I curve. We could see that it maintains fundamental mode condition prior to the local minimum of the slope efficiency. At the place of local minimum, the first high order mode is generated. With increasing current, the intensity of first high order mode increases. On the other hand, the intensity of fundamental mode decreases with the increase in the bias current. Using the illustration of emission spectra of different bias current, we could further understand the effect of SHB and self-focusing on transverse mode of VCSEL device.

4.3 Influence of Temperature on VCSEL Performance

Generally speaking, the most widely recognized limitation on the performance of VCSELs is the generation of heat inside the laser cavity 【38】. Self-heating in VCSELs can be attributed to the excessive heatsource and the accumulation of heat inside the laser cavity. In this section, the thermal roll-over effect, active region temperature, and the dependence of the steady state performance such as threshold current, output power as well as slope efficiency on the temperature of laser cavity are described.

4.3.1 Thermal Roll-Over Effect

When current injection exceeds a certain critical point, output power begins to decrease as the current injection increases. It is shown that the output power is saturated at high injection current. This “roll-over” phenomenon is due to the several effects as follows: (1) the thermal leakage of carriers outside the active region can lead to a reduction of injection efficiency. When the temperature increases, the position of the active layer’s Fermi levels rises relative to the bandgap. Consequently, the active layer becomes decreasingly capable of confining carriers. (2) with increase of the temperature, both the gain spectrum peak as well as the lasing wavelength (i.e. the FP resonance mode) red shift due to changes in bandgap energy of the active region and refractive index of the laser cavity, respectively. The temperature coefficient of the bandgap energy, however, is much greater than that of the refractive index. Consequently, red shift of gain spectrum peak with temperature is much faster than the FP resonance mode. This phenomenon reduces the overlap between the gain peak and the FP resonance mode. Therefore, the output power decreases with increasing the injection current. The scheme of the alignment between the gain peak as well as the FP resonance mode, and the thermal roll-over effect is shown in Figure 4.11.

4.3.2 Determination of Active Region Temperature

In order to understand the influence of temperature on VCSEL device, we calculate the temperature of active region with various bias current, i.e., self-heating in the active region. However, as noted earlier, the FP resonance mode wavelength red shifts with increasing temperature due to increase in the refractive index and is thus a good measure of the active region temperature. We determined the FP mode wavelength, from the peak of the electroluminescence spectrum at a constant injection current, as a function of temperature from 20℃ to 80℃. The electroluminescence spectrum of a 12 μm diameter VCSEL at constant current 10mA, as a function of temperature from 20℃ to 80℃ is shown in Figure 4.12. The FP mode wavelength was observed to increase in average with heat-sink temperature by 0.0556 nm/℃. The shift of the FP mode of lasing wavelength is thus a thermometer of the active region temperature relative to that of the heat-sink at any value of the injection current.

Figure 4.13 shows the electroluminescence spectrum of a 12 μm diameter VCSEL at various bias current values at the heat-sink temperature of 25℃. The measured FP mode wavelength is shown in Figure 4.14. The data for measured FP mode wavelength have been fit with the expression

$$\lambda(I) = \lambda_0 + 0.05I + 0.0255I^2 \qquad \textbf{(4.3)}$$

where I is the bias current in mA, and λ_0 is the FP mode wavelength when the heating is negligible and the active region temperature approaches that of the heat-sink. It is approximately 851.699 nm. Then, from the previously determined temperature coefficient of the FP mode wavelength, the temperature T of the active region at any current I is computed from the emission wavelength.

Figure 4.15(a) shows the CW L-I-V characteristics of a 12 μm diameter VCSEL held at a constant heat-sink temperature of 25℃, and Figure 4.15(b) shows the active region

temperature at various current. In Figure 4.15(b), the solid line through the measured data represents the best fit curve given by

$$T(I) = T_S + 0.873I + 0.461I^2 \quad \textbf{(4.4)}$$

where T_S is the heat-sink temperature and I is the bias current in mA. The active region temperature increases quadratically with the current since it is proportional to the electrical power dissipation.

From Figure 4.15, we observe the VCSEL active region temperature rises from 25℃ to 51.6℃ when it reaches threshold at 6.7 mA. At 13.7 mA for thermal roll-over, the active region temperature has risen by as much as 99℃ above that of the heat-sink to 124℃. The electrical power dissipated at this current is 78.92 mW as obtained from the current-voltage product neglecting the power emitted as light. This suggests rather high thermal impedance, 1254.4 K/W. We believe that such excessive temperature gradients are possible close to the active region due to the much higher current densities used over a relatively small area.

4.3.3 Influence of Temperature on Threshold Current and Output Power

The L-I characteristics of a 12 μm diameter VCSEL under CW current operations for various heat-sink temperatures from 20℃ to 90℃ is shown in Figure 4.16. The variation of threshold current for various heat-sink temperatures is shown in Figure 4.17(a), and the operating current range and maximum output power, as functions of the heat-sink temperature is shown in Figure 4.17(b). We observed that the threshold current, which is dependent on the selection of gain offset wavelength, increases with the increase of temperature. On the other hand, the operating current range and maximum output power both reduce as heat-sink temperature is increased. In addition, the slope efficiency decreases with the increase of temperature, and it is shown in Figure 4.18.

The reason of these phenomena with the change in heat-sink temperature is the same as

that of the thermal roll-over effect. The VCSEL devices are sensitive to the temperature. With increase of the temperature, both the gain spectrum as well as the FP resonance mode red shift due to changes in bandgap energy of the active region and refractive index of the laser cavity, respectively. Consequently, red shift of gain spectrum with temperature is much faster than the FP resonance mode. This phenomenon reduces the overlap between the gain peak and the FP resonance mode. Therefore, the threshold current increases with the increase of the heat-sink temperature. The operating current range, peak output power as well as slope efficiency reduces with the increase of the heat-sink temperature.

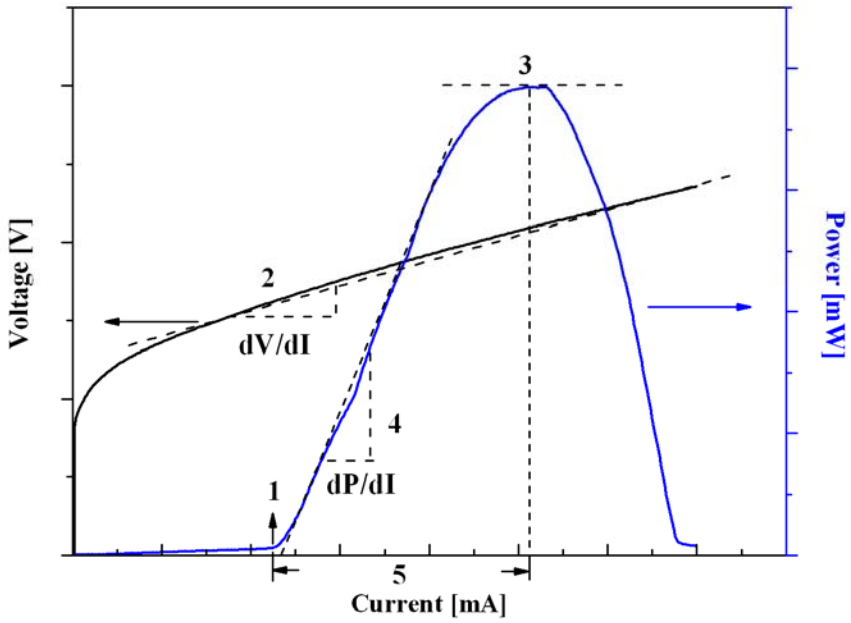

Figure 4.1 Schematic diagram of typical L-I-V characteristics of a VCSEL.

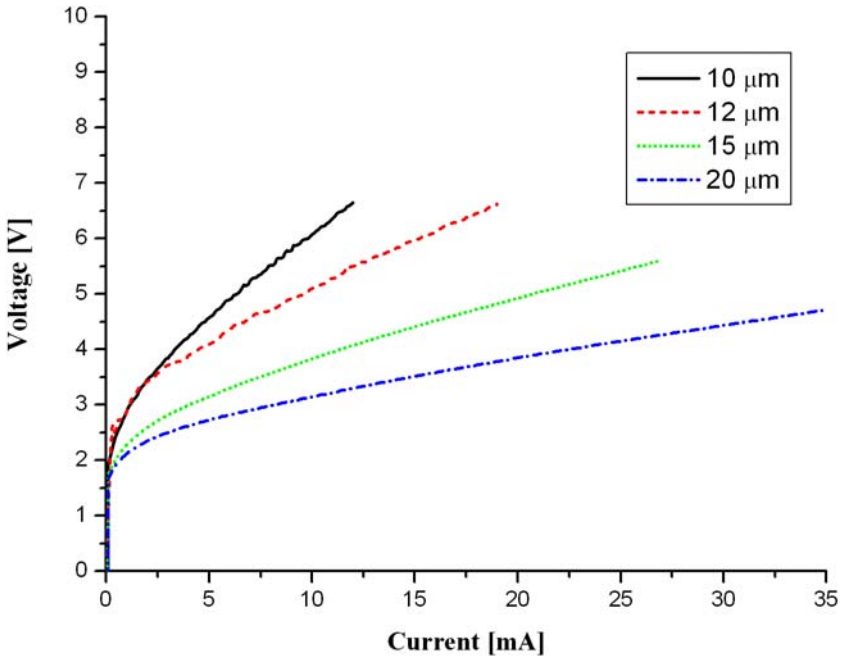

Figure 4.2 The continuous wave I-V characteristics of the devices with different active region diameter.

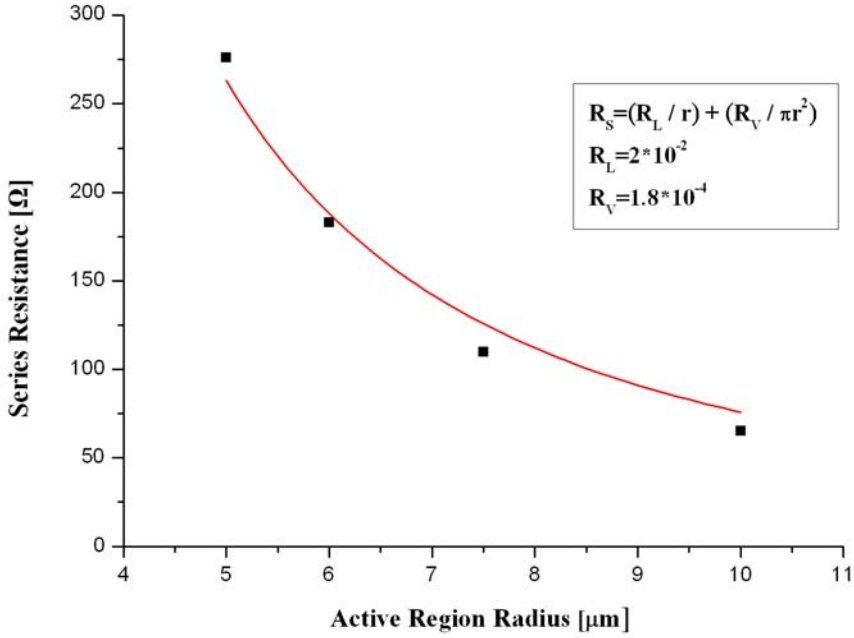

Figure 4.3 The series resistance versus active region radius.

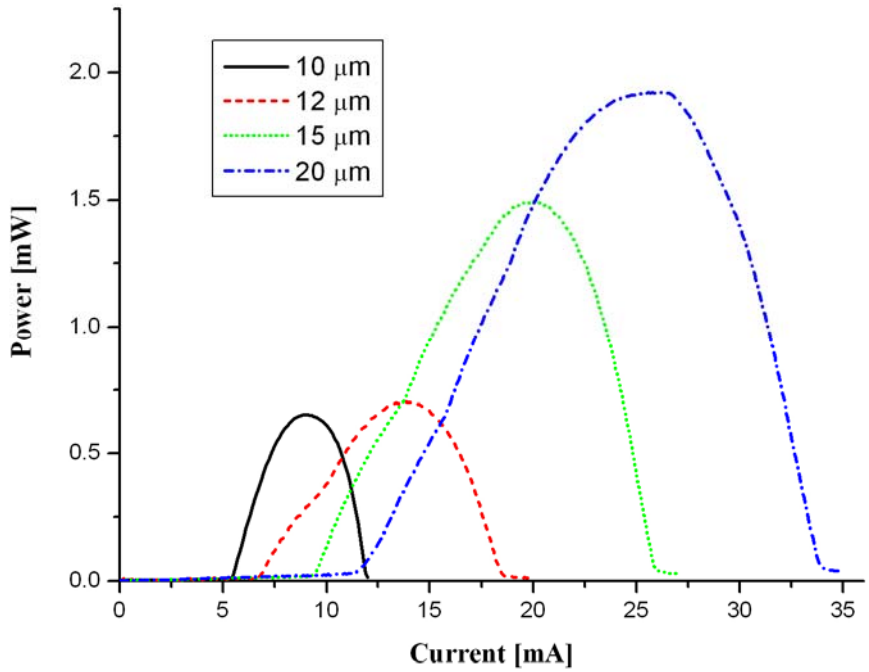

Figure 4.4 The continuous wave L-I characteristics of the devices with different active region diameter.

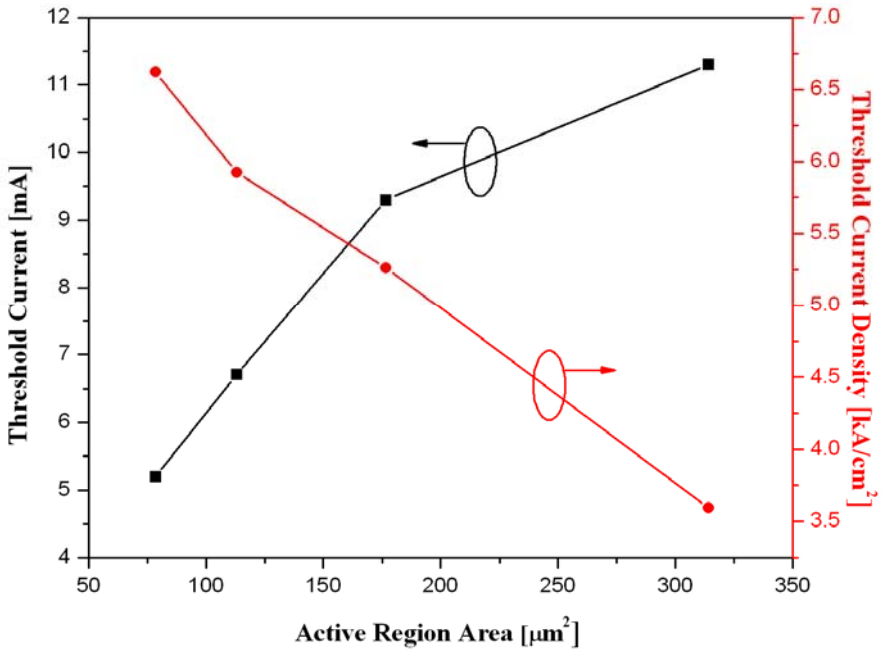

Figure 4.5 The threshold current density and threshold current versus the active region area.

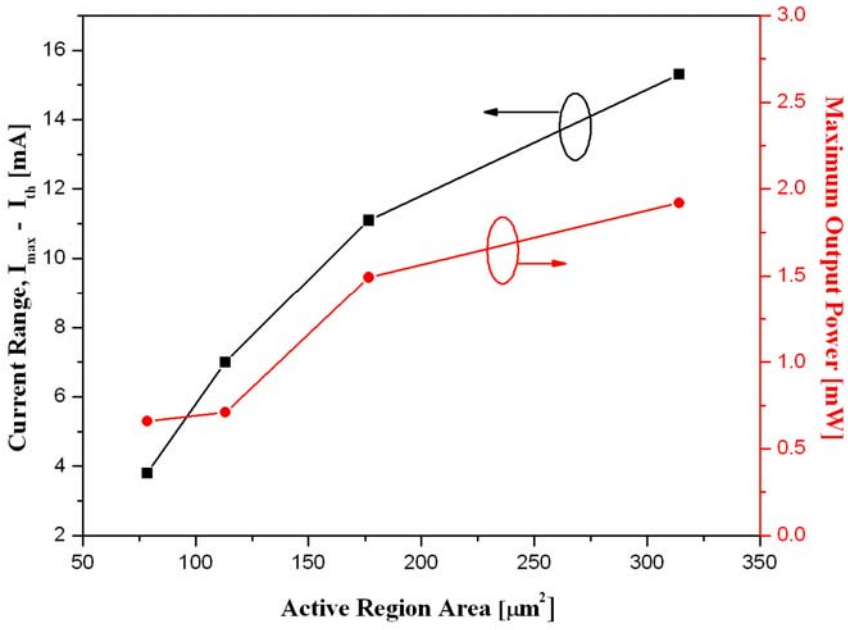

Figure 4.6 Operating current range and maximum output power versus the active region area.

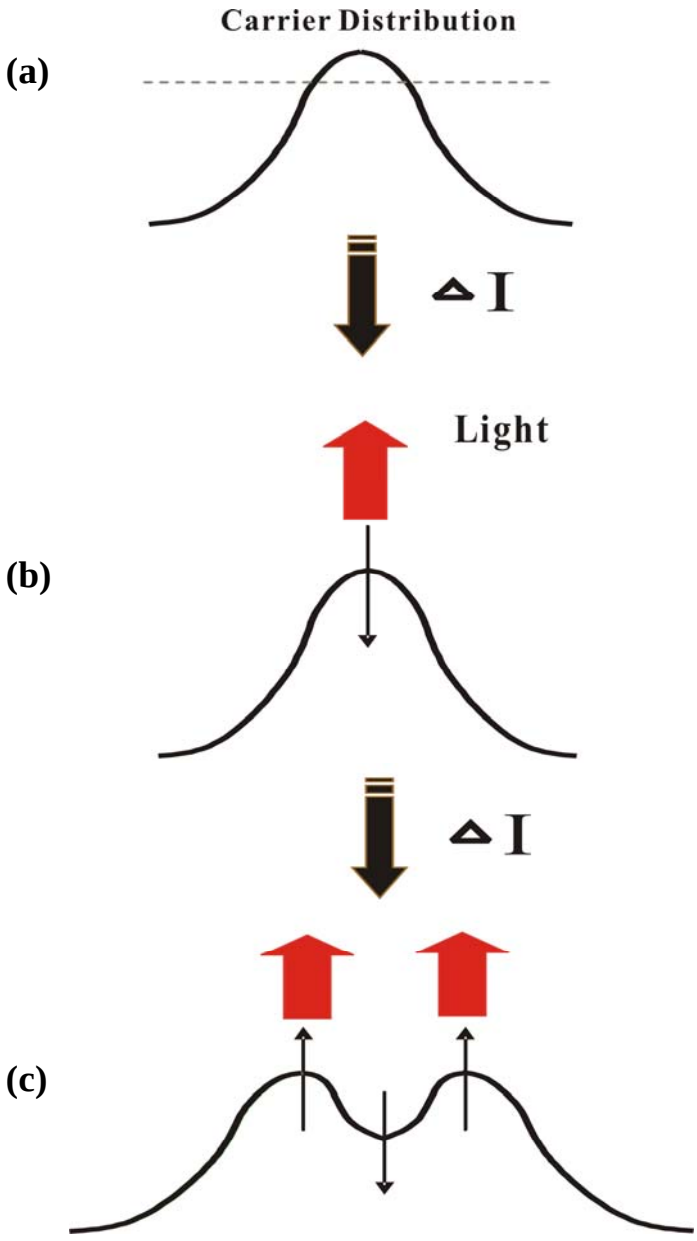

Figure 4.7 The spatial hole burning effect starts with (a) the initial gain above threshold, (b) the increasing intensity of light reduces the gain in the middle along with the injection current, and (c) the gain in the surroundings eventually above threshold and the high order mode starts to lase.

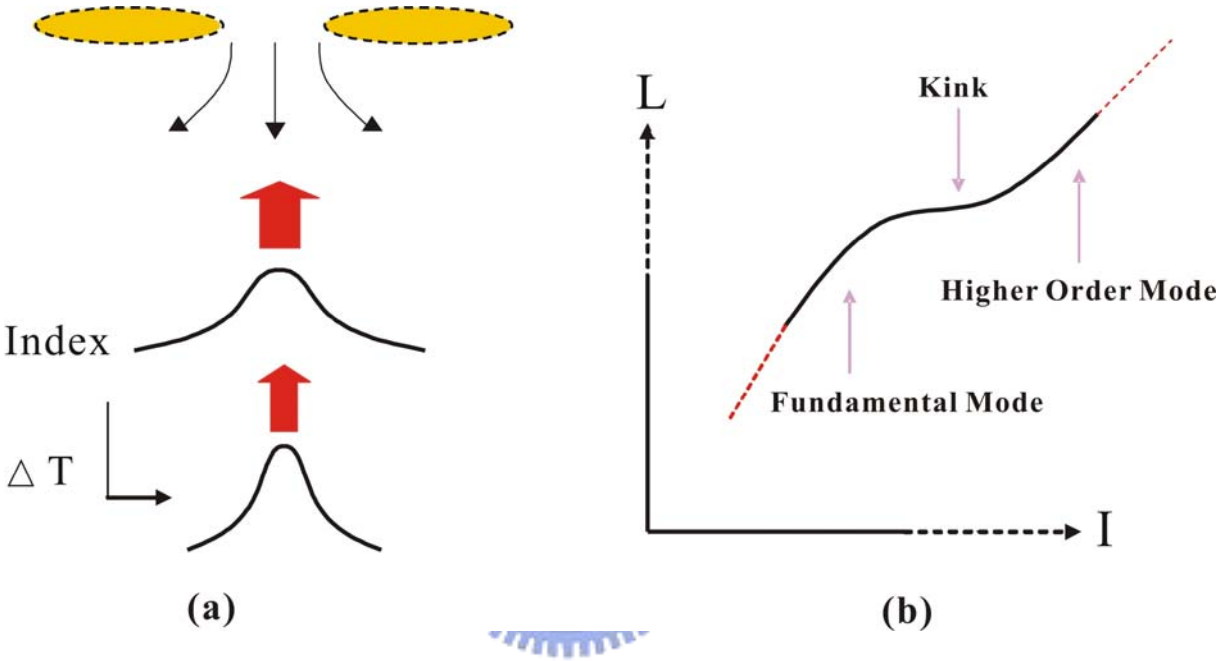

Figure 4.8 (a) The self-focusing effect, and (b) the kink of the L-I curve corresponding to the transverse mode formation.

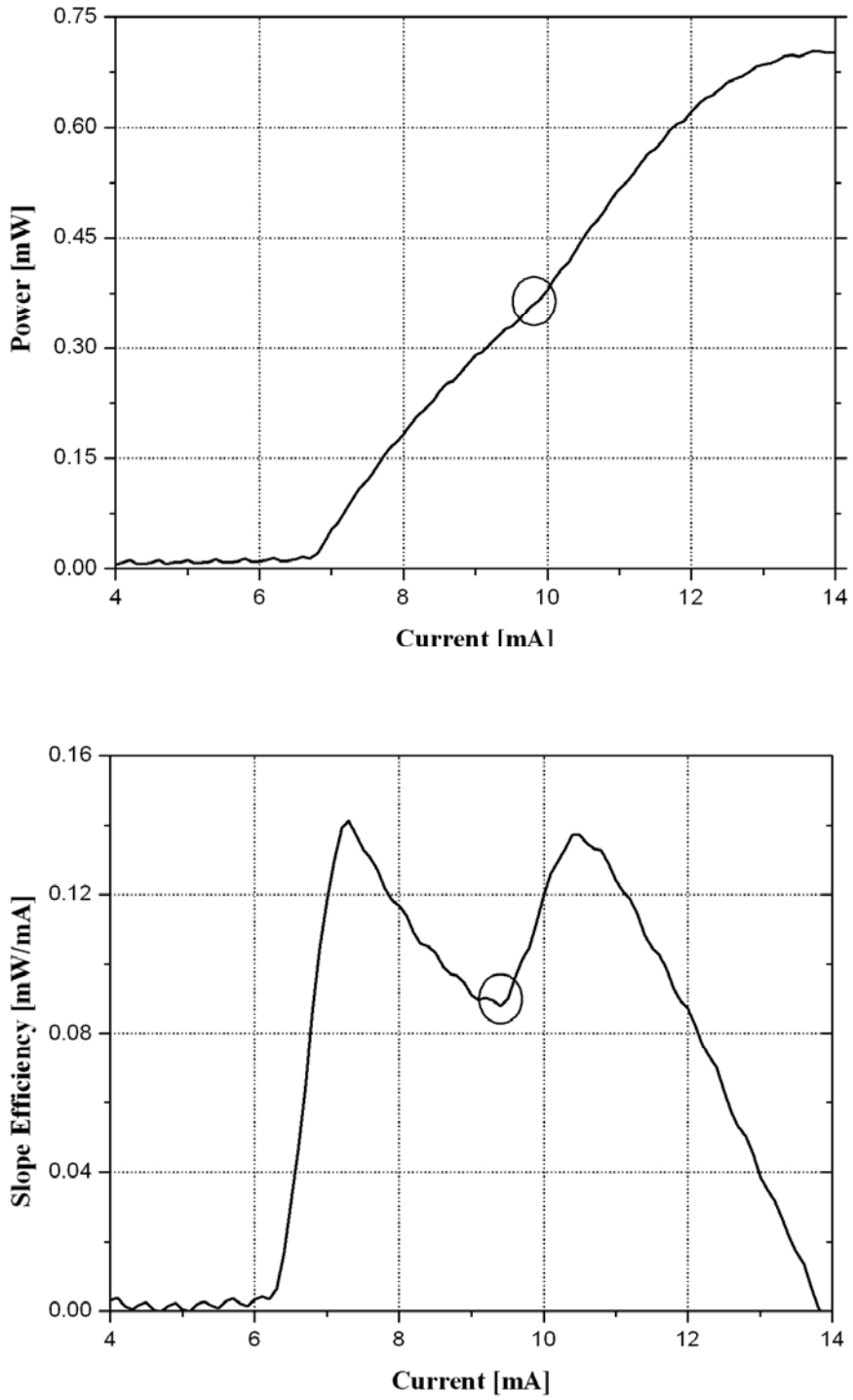

Figure 4.9 The slope efficiency in relation to the kink in the L-I curve.

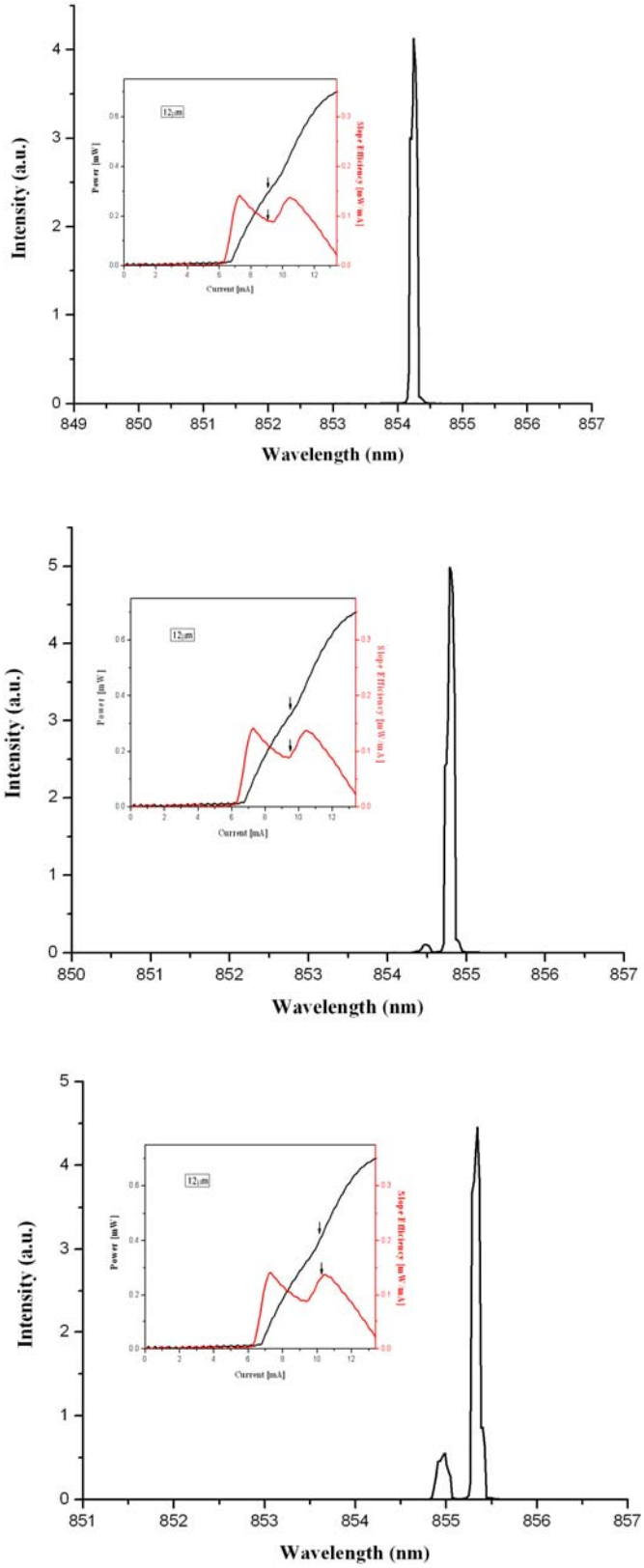

Figure 4.10 The emission spectra in the vicinity of the kink in L-I curve.

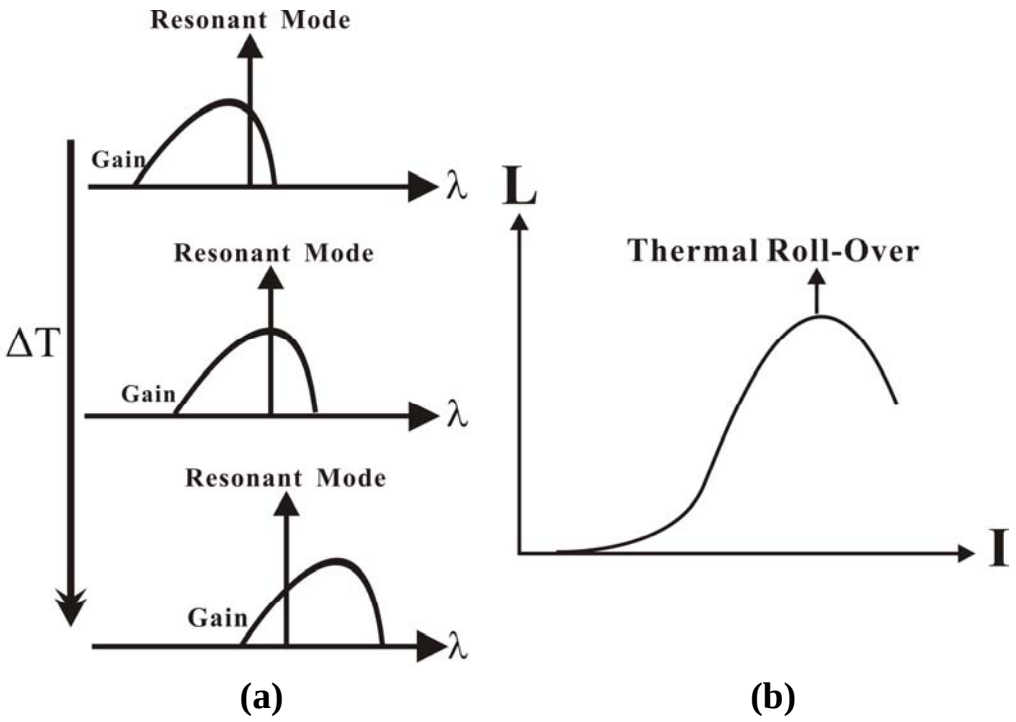

Figure 4.11 (a) The scheme of the alignment between the gain peak as well as the FP resonance mode, and (b) the thermal roll-over effect.

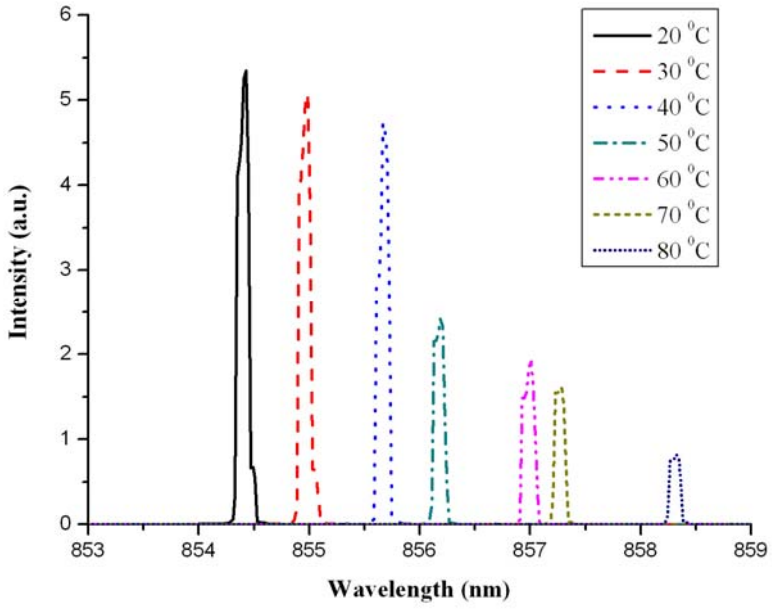

Figure 4.12 The electroluminescence spectrum of a 12 μm diameter VCSEL at constant current 10mA, as a function of temperature from 20℃ to 80℃.

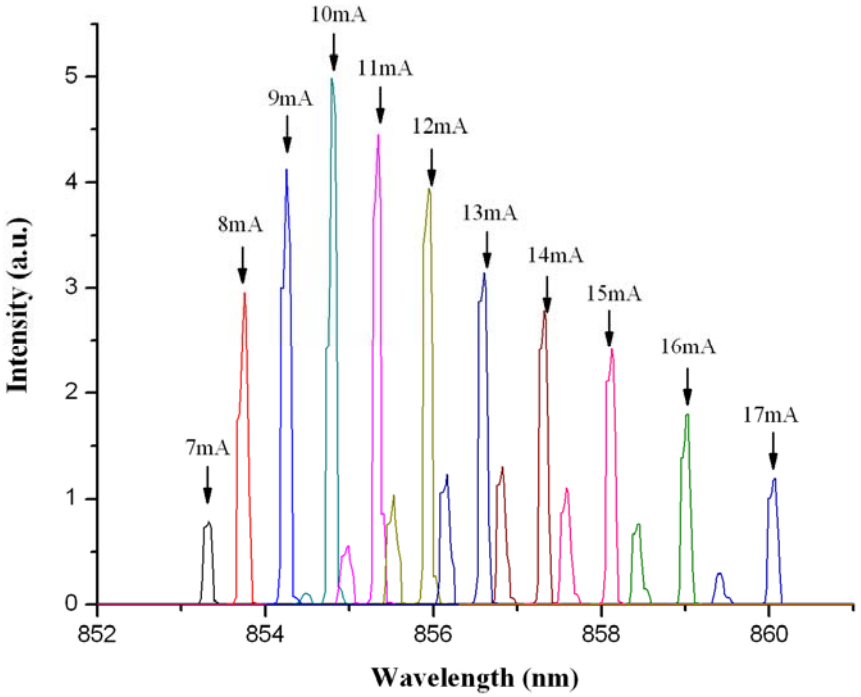

Figure 4.13 The electroluminescence spectrum of a 12 μm diameter VCSEL at various bias current values at the heat-sink temperature of 25℃.

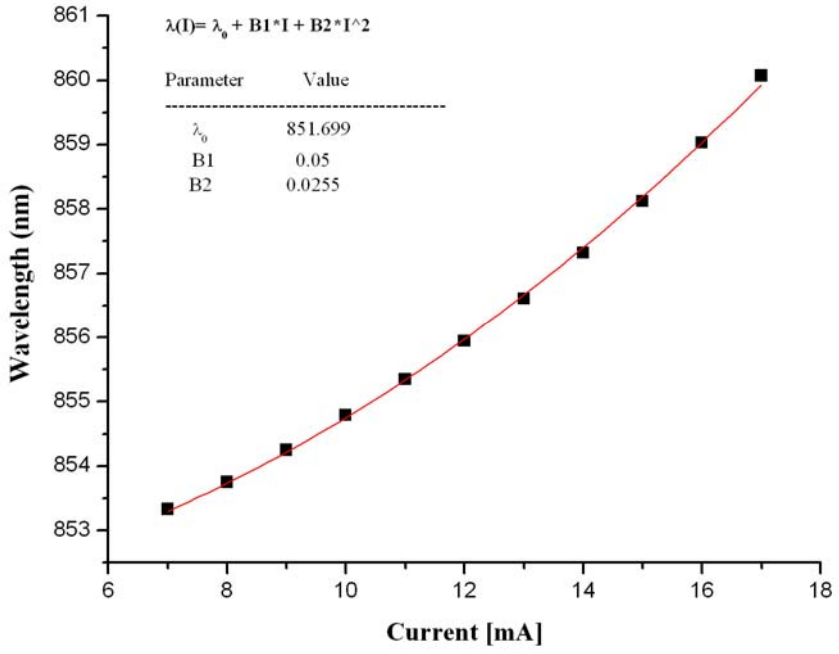

Figure 4.14 The measured FP mode wavelengths at various bias current values.

(a)

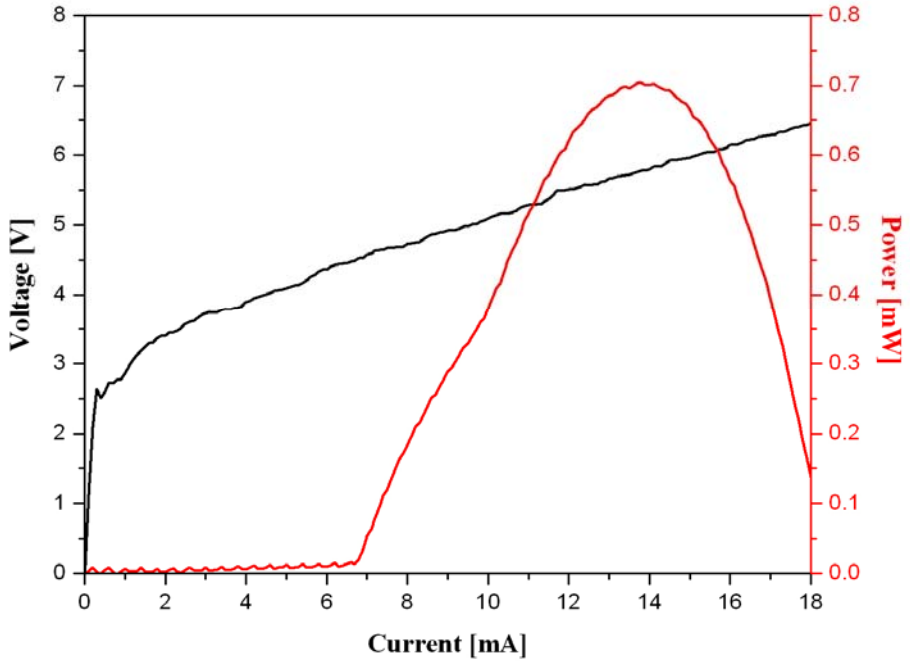

(b)

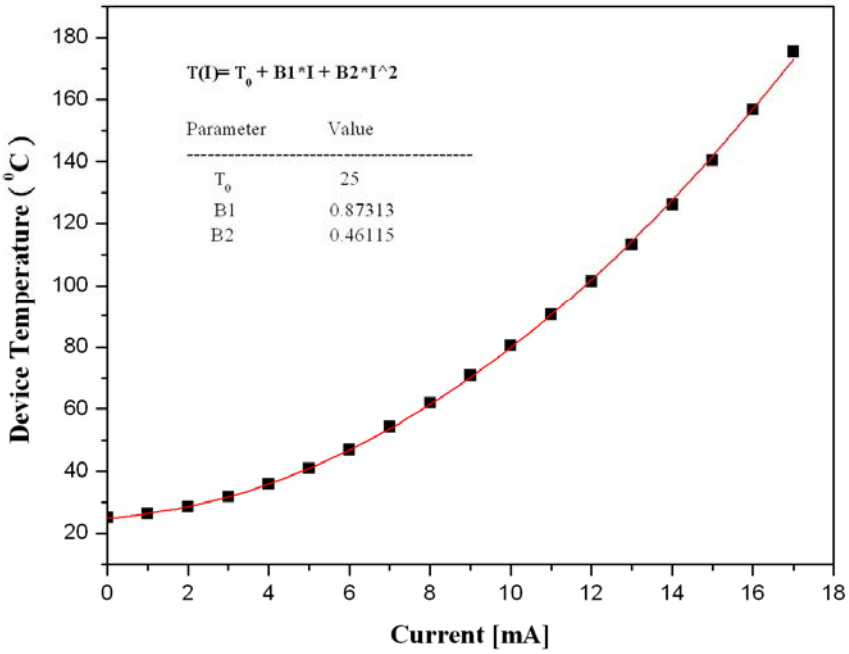

Figure 4.15 (a) The CW L-I-V characteristics of a 12 μm diameter VCSEL at a constant heat-sink temperature of 25℃, and (b) the corresponding active region temperature at various current.

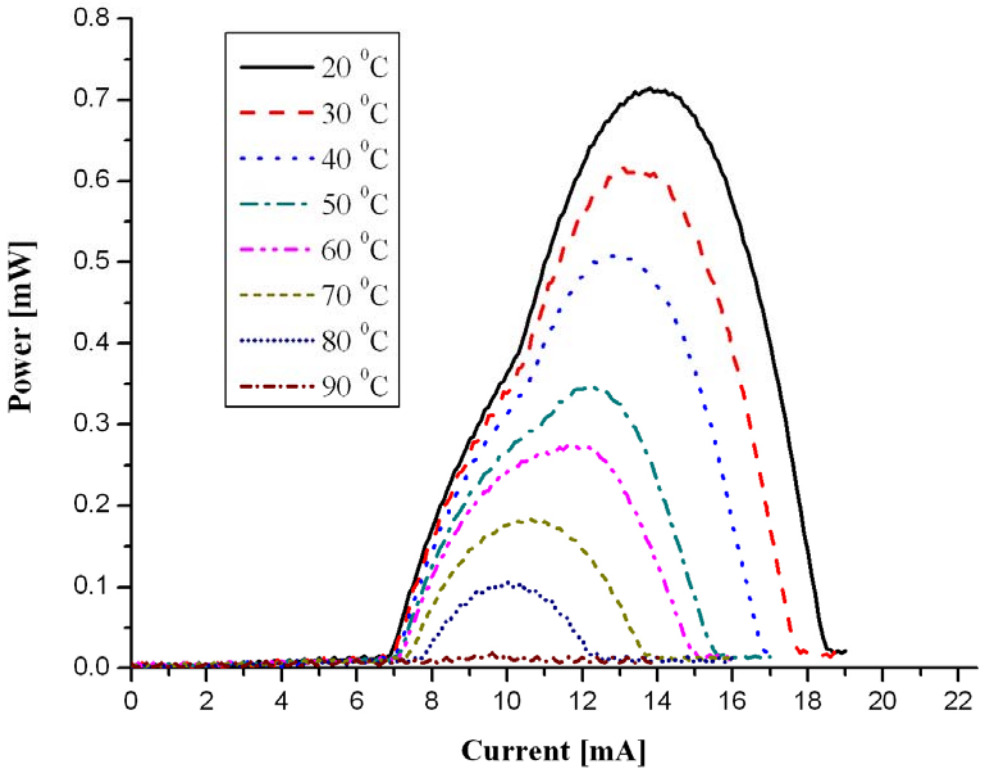

Figure 4.16 The L-I characteristics of a 12 μm diameter VCSEL under CW current operations for various heat-sink temperatures from 20℃ to 90℃.

(a)

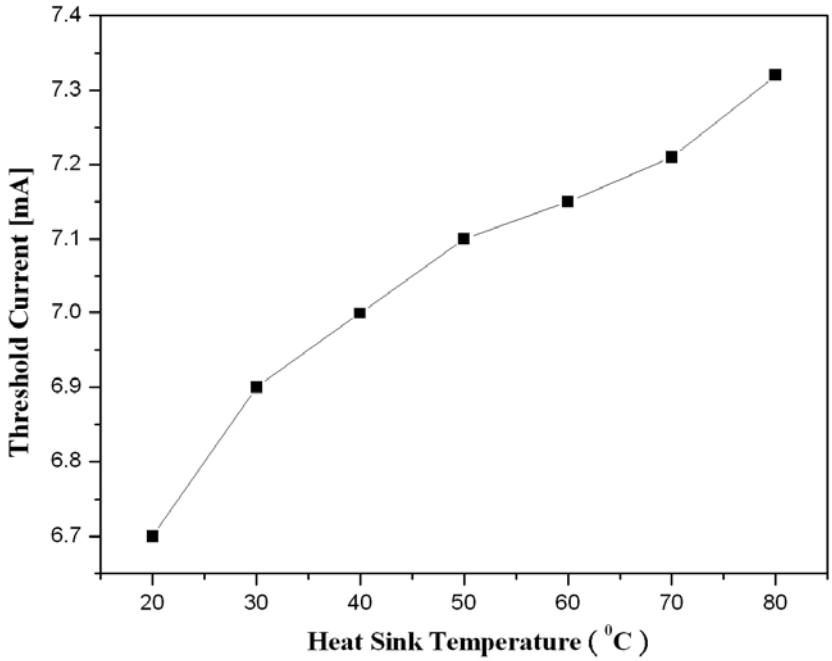

(b)

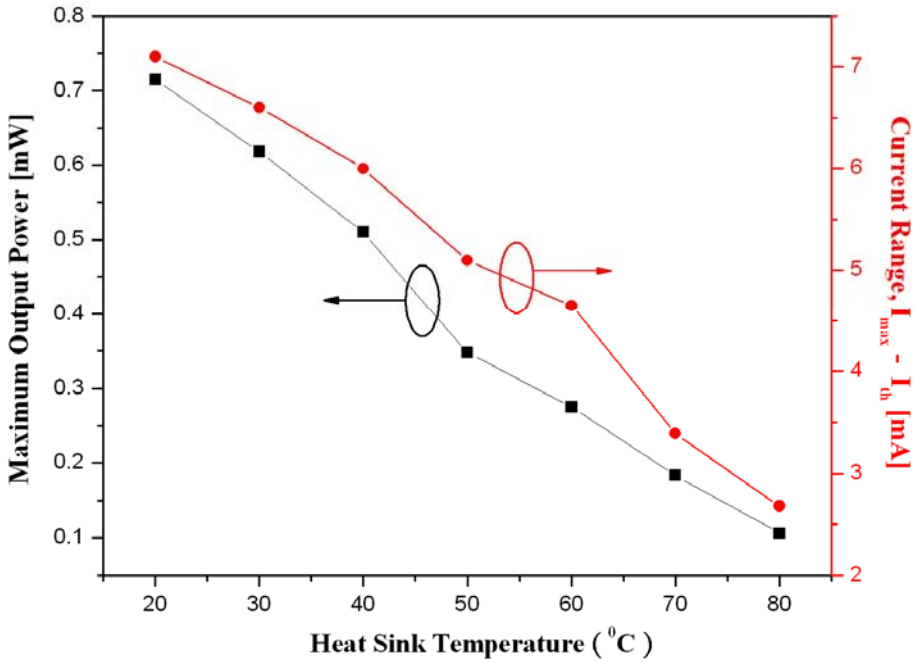

Figure 4.17 (a) The variation of threshold current for various heat-sink temperatures, and (b) the operating current range and maximum output power, as functions of the heat-sink temperature.

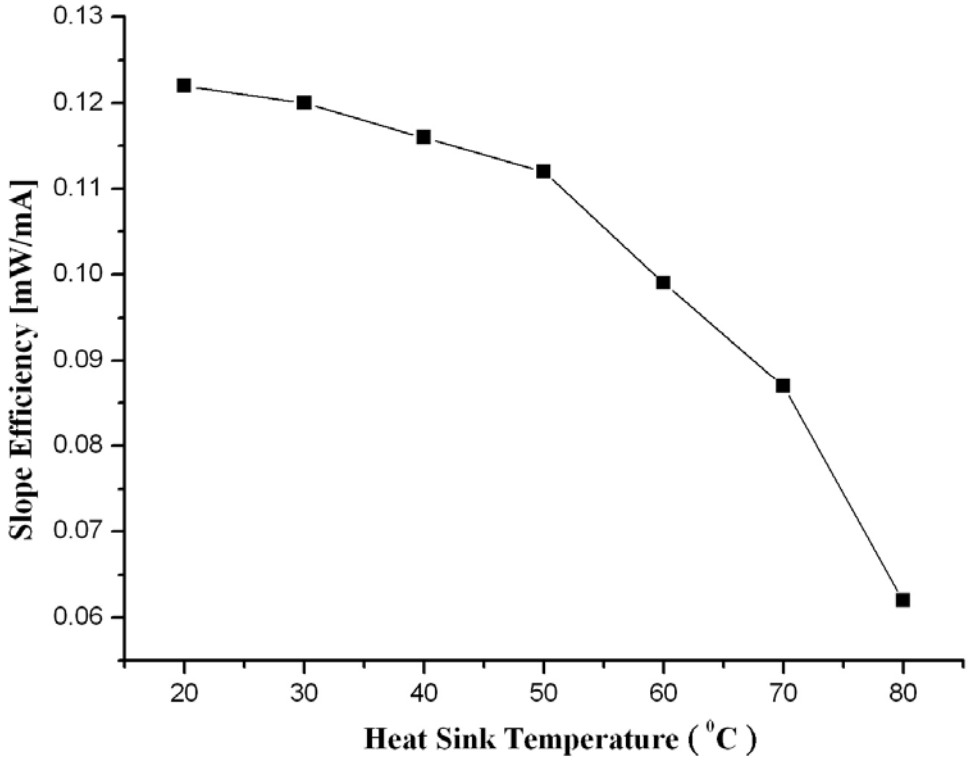

Figure 4.18 The slope efficiency, as functions of the heat-sink temperature.